Inorg. Chem. **2009**, *48*, 2956−2966

Cyanide-Bridged $Fe^{III}-Mn^{III}$ Bimetallic Complexes with Dimeric and Chain Structures Constructed from a Newly Made *mer*-Fe Tricyanide: Structures and Magnetic Properties

Jae Il Kim,[†] Hyun Young Kwak,[†] Jung Hee Yoon,[†] Dae Won Ryu,[†] In Young Yoo,[†] Namgeun Yang,[‡] Beong Ki Cho,[§] Je-Geun Park,[‡] Hyosug Lee,[||] and Chang Seop Hong*[,†]

Department of Chemistry, Korea University, Seoul 136-713, Korea, Department of Physics and Department of Energy Science, SungKyunKwan University, Suwon 440-746, Korea, Department of Materials Science and Engineering, GIST, Gwangju 500-712, Korea, and Hybrid Materials Group, Materials Research Laboratory, SAIT, Yongin-City 446-712, Korea

Received October 23, 2008

Four cyanide-linked $Fe^{III}-Mn^{III}$ complexes were prepared by reacting Mn Schiff bases with a new molecular precursor $(PPh_4)[Fe(qcq)(CN)_3]$ [**1**; qcq = 8-(2-quinolinecarboxamido)quinoline anion]. They include a dimeric molecule, $[Fe(qcq)(CN)_3][Mn(3\text{-}MeOsalen)(H_2O)]\cdot 2H_2O$ [**2**$\cdot 2H_2O$; 3-MeOsalen = N,N′-ethylenebis(3-methoxysalicylideneiminato) dianion], and three 1D zigzag chains, $[Fe(qcq)(CN)_3][Mn(5\text{-}Clsalen)]\cdot 3H_2O$ [**3**$\cdot$2MeOH; 5-Clsalen = N,N′-ethylenebis(5-chlorosalicylideneiminato) dianion], $[Fe(qcq)(CN)_3][Mn(5\text{-}Brsalen)]\cdot$2MeOH [**4**$\cdot$2MeOH; 5-Brsalen = N,N′-ethylenebis(5-bromosalicylideneiminato) dianion], and $Fe(qcq)(CN)_3][Mn(salen)]\cdot MeCN\cdot H_2O$ [**5**$\cdot$MeCN; salen = N,N′-ethylenebis(salicylideneiminato) dianion]. The complexes consist of extensive hydrogen bonding and $\pi-\pi$ stacking interactions, generating multidimensional structures. Magnetic studies demonstrate that antiferromagnetic couplings are operative between Fe^{III} and Mn^{III} centers bridged by cyanide ligands. On the basis of an infinite chain model, magnetic coupling parameters of **2**−**5** range from −9.3 to −14.1 cm^{-1}. A long-range order is observed at 2.3 K for **3** and 2.2 K for **4**, while compound **5** shows spin glass behavior possibly coupled with magnetic ordering.

Introduction

The research on molecule-based magnetic materials has attracted much attention because of the materials' potential applications in magnetic devices.[1] In particular, cyanide-bridged magnetic complexes have been intensively studied in view of intriguing multifunctional magnetic characters.[2−4] A variety of molecular units, hexacyanometalates or octacyanometalates, have been utilized as synthons to build discrete molecules or coordination networks.[2−6] In this case, the structural dimensionality can be controlled depending on experimental conditions and counterparts used.

Recently, low-dimensional magnetic systems with an anisotropic nature have been one of the hot issues among molecule-based magnetic materials. Single-molecule magnets (SMMs) exhibit peculiar slow magnetic relaxation and quantum tunneling of magnetization below a blocking temperature.[7] Another attractive challenge has been in regards to the design and fabrication of single-chain magnets (SCMs), which display the same relaxation effects on magnetization.[8] The construction of such low-dimensional systems can be more reliably achieved by taking advantage

* To whom correspondence should be addressed. E-mail: cshong@korea.ac.kr.
[†] Korea University.
[‡] SungKyunKwan University.
[§] GIST.
[||] SAIT.

(1) Turnbull, M. M.; Sugimoto, T.; Thompson, L. K. *Molecule-Based Magnetic Materials*; American Chemical Society: Washington, DC, 1996.
(2) Coronado, E.; Palacio, F.; Veciana, J. *Angew. Chem., Int. Ed.* **2003**, *42*, 2570.
(3) (a) Dei, A. *Angew. Chem., Int. Ed.* **2005**, *44*, 1160. (b) Arimoto, Y.; Ohkoshi, S.-i.; Zhong, Z. J.; Seino, H.; Mizobe, Y.; Hashimoto, K. *J. Am. Chem. Soc.* **2003**, *125*, 9240. (c) Herrera, J. M.; Marvaud, V.; Verdaguer, M.; Marrot, J.; Kalisz, M.; Mathonière, C. *Angew. Chem., Int. Ed.* **2004**, *43*, 5468. (d) Ohkoshi, S.-i.; Tokoro, H.; Hozumi, T. Z. Y.; Hashimoto, K.; Mathonière, C.; Bord, I.; Rombaut, G.; Verlelst, M.; Moulin, C. C. d.; Villain, F. *J. Am. Chem. Soc.* **2006**, *128*, 270. (e) Ohkoshi, S.-i.; Ikeda, S.; Hozumi, T.; Kashiwagi, T.; Hashimoto, K. *J. Am. Chem. Soc.* **2006**, *128*, 5320.
(4) (a) Inoue, K.; Kikuchi, K.; Ohba, M.; Okawa, H. *Angew. Chem., Int. Ed.* **2003**, *42*, 4810. (b) Kaneko, W.; Kitagawa, S.; Ohba, M. *J. Am. Chem. Soc.* **2007**, *129*, 248. (c) Imai, H.; Inoue, K.; Kikuchi, K.; Yoshida, Y.; Ito, M.; Sunahara, T.; Onaka, S. *Angew. Chem., Int. Ed.* **2004**, *43*, 5618.

10.1021/ic802033q CCC: $40.75

Published on Web 02/27/2009

of capped molecular precursors $[Fe(L)(CN)_x]^{y-}$ (L = blocking ligands, $x = 2-5$) with magnetic anisotropy rather than using the nonblocked cyanide precursors. The molecule-level magnets, however, require magnetic anisotropic spin centers incorporated into molecular units at least, as well as negligible intermolecular interaction between molecules or chains with respect to intramolecular interaction. When the intermolecular interaction becomes significant, the intrinsic magnetic characters of SMMs and SCMs smear out. For instance, the presence of sizable intermolecular contacts (hydrogen bonding, $\pi-\pi$ interactions, and so on) allowed for magnetic systems with field-induced metamagnetic transition or long-range magnetic ordering.[9] Some low-dimensional assemblies (clusters and chains) showed three-dimensional (3D) magnetic arrangements and revealed a degree of magnetic glassy state at the same time.[10]

Among the precursors $[Fe(L)(CN)_x]^{y-}$, molecular building bricks with L = tridentate ligand and $x = 3$ can have facial and meridional configurations relying on the relative disposition of the three cyanide groups around the Fe^{III} center. Facial Fe^{III} tricyanide precursors with blocking groups, hydrotris(pyrazolyl)borate (Tp), hydrotris(3,5-dimethylpyrazol-1-yl)borate (Tp*), tetra(pyrazol-1-yl)borate (pzTp), and 1,3,5-triaminocyclohexane (tach), were frequently utilized to generate a number of magnetic systems with molecular and 1D chain structures.[11] On the contrary, magnetic entities fabricated by *mer*-$[Fe^{III}(L)(CN)_3]^-$ are still limited; they contain chelating ligands, bis(2-pyridylcarbonyl)amidate anion (bpca),[12] 8-(pyridine-2-carboxamido)quinoline anion (pcq),[13] 8-(pyrazine-2-carboxamido)quinoline anion (pzcq),[14] and 8-(5-methylpyrazine-2-carboxamido)quinoline anion (mpzcq).[15] However, to date, only a few Mn(II)−Fe(III) and Mn(III)−Fe(III) bimetallic complexes based on *mer*-Fe^{III} cyanides were characterized structurally and magnetically.[12−15]

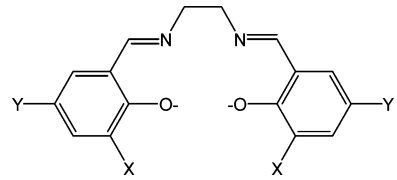

2: 3-MeOsalen: X = OCH_3, Y = H
3: 5-Clsalen: X = H, Y = Cl
4: 5-Brsalen: X = H, Y = Br
5: salen: X = H, Y = H

Herein, we report the syntheses, structures, and magnetic properties of a dimer, $[Fe(qcq)(CN)_3][Mn(3\text{-}MeOsalen)(H_2O)]\cdot 2H_2O$ [**2**·$2H_2O$; 3-MeOsalen = N,N′-ethylenebis(3-methoxysalicylideneiminato) dianion], and three one-dimensional (1D) zigzag chains, $[Fe(qcq)(CN)_3][Mn(5\text{-}Clsalen)]\cdot 3H_2O$ [**3**·2MeOH; 5-Clsalen = N,N′-ethylenebis(5-chlorosalicylideneiminato) dianion], $[Fe(qcq)(CN)_3][Mn(5\text{-}Brsalen)]\cdot 2MeOH$ [**4**·2MeOH; 5-Brsalen = N,N′-ethylenebis(5-bromosalicylideneiminato) dianion], and $Fe(qcq)(CN)_3][Mn(salen)]\cdot MeCN\cdot H_2O$ [**5**·MeCN; salen = N,N′-ethylenebis(salicylideneiminato) dianion], using a newly designed molecular precursor $(PPh_4)[Fe(qcq)(CN)_3]$ [**1**; qcq = 8-(2-quinolinecarboxamido)quinoline anion]. Their crystal packing diagrams are composed of extensive noncovalent forces such as hydrogen bonding and $\pi-\pi$ contacts, thus affording higher-dimensional structures. Magnetic data show that antiferromagnetic interactions are present between magnetic centers through cyanide bridges in **2**−**5**, which are in contrast with most cyanide-linked $Fe^{III}-Mn^{III}$ bimetallic systems.

Experimental Section

Reagents. Mn Schiff bases were synthesized according to a modified literature procedure.[16] All chemicals and solvents in the synthesis were of reagent grade and used as received. All manipulations were performed under aerobic conditions.

(5) (a) Bennett, M. V.; Long, J. R. *J. Am. Chem. Soc.* **2003**, *125*, 2394. (b) Pradhan, R.; Desplanches, C.; Guionneau, P.; Sutter, J.-P. *Inorg. Chem.* **2003**, *42*, 6607. (c) Shores, M. P.; Sokol, J. J.; Long, J. R. *J. Am. Chem. Soc.* **2002**, *124*, 2279. (d) Ruiz, E.; Rodríguez-Fortea, A.; Alvarez, S.; Verdaguer, M. *Chem.—Eur. J.* **2005**, *11*, 2135. (e) Visinescu, D.; Desplanches, C.; Imaz, I.; Bahers, V.; Pradhan, R.; Villamena, F. A.; Guionneau, P.; Sutter, J.-P. *J. Am.Chem. Soc.* **2006**, *128*, 10202. (f) Lim, J. H.; You, Y. S.; Yoo, H. S.; Yoon, J. H.; Kim, J. I.; Koh, E. K.; Hong, C. S. *Inorg. Chem.* **2007**, *46*, 10578. (g) Lim, J. H.; Kang, J. S.; Kim, H. C.; Koh, E. K.; Hong, C. S. *Inorg. Chem.* **2006**, *45*, 7821. (h) You, Y. S.; Yoon, J. H.; Lim, J. H.; Kim, H. C.; Hong, C. S. *Inorg. Chem.* **2005**, *44*, 7063. (i) You, Y. S.; Kim, D.; Do, Y.; Oh, S. J.; Hong, C. S. *Inorg. Chem.* **2004**, *43*, 6899.

(6) (a) Zhong, Z. J.; Seino, H.; Mizobe, Y.; Hidai, M.; Fujishima, A.; Ohkoshi, S.-i.; Hashimoto, K. *J. Am. Chem. Soc.* **2000**, *122*, 2952. (b) Song, Y.; Zhang, P.; Ren, X.-M.; Shen, X.-F.; Li, Y.-Z.; You, X.-Z. *J. Am. Chem. Soc.* **2005**, *127*, 3708. (c) Lim, J. H.; Yoon, J. H.; Kim, H. C.; Hong, C. S. *Angew. Chem., Int. Ed.* **2006**, *45*, 7424. (d) Freedman, D. E.; Bennett, M. V.; Long, J. R. *Dalton Trans.* **2006**, 2829. (e) Bonadio, F.; Gross, M.; Stoeckli-Evans, H.; Decurtins, S. *Inorg. Chem.* **2002**, *41*, 5891.

(7) Gatteschi, D.; Sessoli, R. *Angew. Chem., Int. Ed.* **2003**, *42*, 268.

(8) (a) Lescouëzec, R.; Toma, L. M.; Vaissermann, J.; Verdaguer, M.; Delgado, F. S.; Ruiz-Pérez, C.; Lloret, F.; Julve, M. *Coord. Chem. Rev.* **2005**, *249*, 2691. (b) Clerac, R.; Miyasaka, H.; Yamashita, M.; Coulon, C. *J. Am. Chem. Soc.* **2002**, *124*, 12837. (c) Coulon, C.; Miyasaka, H.; Clérac, R. *Struct. Bonding (Berlin)* **2006**, *122*, 163.

(9) (a) Yoon, J. H.; Lim, J. H.; Choi, S. W.; Kim, H. C.; Hong, C. S. *Inorg. Chem.* **2007**, *46*, 1529. (b) Wang, S.; Ferbinteanu, M.; Yamashita, M. *Inorg. Chem.* **2007**, *46*, 610. (c) Ni, W.-W.; Ni, Z.-H.; Cui, A.-L.; Liang, X.; Kou, H.-Z. *Inorg. Chem.* **2007**, *46*, 22. (d) Matsumoto, N.; Sunatsuki, Y.; Miyasaka, H.; Hashimoto, Y.; Luneau, D.; Tuchagues, J.-P. *Angew. Chem., Int. Ed.* **1999**, *38*, 171.

(10) (a) Wang, Z.-X.; Li, X.-L.; Wang, T.-W.; Li, Y.-Z.; Ohkoshi, S.-i.; Hashimoto, K.; Song, Y.; You, X.-Z. *Inorg. Chem.* **2007**, *46*, 10990. (b) Liu, W.; Wang, C.-F.; Li, Y.-Z.; Zuo, J.-L.; You, X.-Z. *Inorg. Chem.* **2006**, *45*, 10058. (c) Liu, X.-T.; Wang, X.-Y.; Zhang, W.-X.; Cui, P.; Gao, S. *Adv. Mater.* **2006**, *18*, 2852. (d) Kim, J.; Han, S.; Pokhodnya, K. I.; Migliori, J. M.; Miller, J. S. *Inorg. Chem.* **2005**, *44*, 6983. (e) Li, D.-F.; Zheng, L.-M.; Zhang, T.-Z.; Huang, J.; Gao, S.; Tang, W.-X. *Inorg. Chem.* **2003**, *42*, 6123. (f) Boskovic, C.; Bircher, R.; Tregenna-Piggott, P. L. W.; Gudel, H. U.; Paulsen, C.; Wernsdorfer, W.; Barra, A.-L.; Khatsko, E.; Neels, A.; Stoeckli-Evans, H. *J. Am. Chem. Soc.* **2003**, *125*, 14046.

(11) (a) Liu, W.; Wang, C.-F.; Li, Y.-Z.; Zuo, J.-L.; You, X.-Z. *Inorg. Chem.* **2006**, *45*, 10058. (b) Wen, H.-R.; Wang, C.-F.; Song, Y.; Gao, S.; Zuo, J.-L.; You, X.-Z. *Inorg. Chem.* **2006**, *45*, 8942. (c) Gu, Z.-G.; Yang, Q.-F.; Liu, W.; Song, Y.; Li, T.-Z.; Zuo, J.-L.; You, X.-Z. *Inorg. Chem.* **2006**, *45*, 8895. (d) Wang, S.; Zuo, J.-L.; Zhou, H.-C.; Choi, H. J.; Ke, Y.; Long, J. R.; You, X.-Z. *Angew. Chem., Int. Ed.* **2004**, *43*, 5940. (e) Li, D.; Parkin, S.; Wang, G.; Yee, G. T.; Prosvirin, A. V.; Holmes, S. M. *Inorg. Chem.* **2005**, *44*, 4903. (f) Li, D.; Parkin, S.; Wang, G.; Yee, G. T.; Clérac, R.; Wernsdorfer, W.; Holmes, S. M. *J. Am. Chem. Soc.* **2006**, *128*, 4214. (g) Yang, J. Y.; Shores, M. P.; Sokol, J. J.; Long, J. R. *Inorg. Chem.* **2003**, *42*, 1403. (h) Wang, S.; Zuo, J.-L.; Gao, S.; Song, Y.; Zhuo, H.-C.; Zhang, Y.-Z.; You, X.-Z. *J. Am. Chem. Soc.* **2004**, *126*, 8900.

(12) Lescouëzec, R.; Vaissermann, J.; Toma, M.; Carrasco, R.; Lloret, F.; Julve, M. *Inorg. Chem.* **2004**, *43*, 2234.

(13) Ni, Z.-H.; Kou, H.-Z.; Zhang, L.-F.; Ni, W.-W.; Jiang, Y.-B.; Cui, A.-L.; Ribas, J.; Sato, O. *Inorg. Chem.* **2005**, *44*, 9631.

(14) Kim, J. I.; Yoo, H. S.; Koh, E. K.; Kim, H. C.; Hong, C. S. *Inorg. Chem.* **2007**, *46*, 8481.

(15) Kim, J. I.; Yoo, H. S.; Koh, E. K.; Hong, C. S. *Inorg. Chem.* **2007**, *46*, 10461.

(16) Karmakar, R.; Choudhury, C. R.; Bravic, G.; Sutter, J.-P.; Mitra, S. *Polyhedron* **2004**, *23*, 949.

Synthesis. ***Caution!*** *Perchlorate salts of metal compounds with organic ligands are potentially explosive, and cyanides are toxic. These materials should be handled with great caution.*

8-(2-Quinolinecarboxamido)quinoline (Hqcq). Quninaldic acid (0.020 mol) and 8-aminoquinoline (0.020 mol) in pyridine (15 mL) were stirred with heating up to 100 °C. Triphenyl phosphite (0.020 mol) was added to the resultant mixture and stirred at 100 °C for 4 h. The deep brown solution was cooled to room temperature and concentrated in a vacuum. Crystalline solids were formed by adding EtOH. The solids were collected with filtration, washed with EtOH, and air-dried. Yield: 43%. Elem anal. (%) calcd for $C_{19}H_{13}N_3O$: C, 76.2; H, 4.38; N, 14.0. Found: C, 76.4; H, 4.16; N, 13.9.

Fe(qcq)Cl$_2$. To $FeCl_3 \cdot 6H_2O$ (8.54 mmol) in MeOH (60 mL) were added Hqcq (8.54 mmol) and NaOH (8.54 mmol). The reaction mixture was refluxed for 3 h, forming deep-green crystalline powders. The product was obtained with filtration and air-dried. Yield: 85%. Elem anal. (%) calcd for $C_{19}H_{12}Cl_2FeN_3O$: C, 53.7; H, 2.85; N, 9.89. Found: C, 53.9; H, 2.87; N, 9.56.

K[Fe(qcq)(CN)$_3$]. To a suspension of Fe(qcq)Cl$_2$ (7.52 mmol) in MeOH was slowly added KCN (22.5 mmol). The mixture was refluxed for 3 h, precipitating dark-brown powders, which were dried in a vacuum. The crude solids were recrystallized in MeOH. Yield: 46%.

(PPh$_4$)[Fe(qcq)(CN)$_3$] (1). PPh_4Br (1.2 mmol) dissolved in H_2O was added to K[Fe(qcq)(CN)$_3$] (1.0 mmol) in H_2O. Immediately, brown powders were precipitated, which were filtered and air-dried. The recrystallization was conducted by a MeOH/ether solvent pair. Yield: 72%. Elem anal. (%) calcd for $C_{46}H_{32}FeN_6OP$: C, 71.6; H, 4.18; N, 10.9. Found: C, 71.6; H, 4.25; N, 10.7.

[Fe(qcq)(CN)$_3$][Mn(3-MeOsalen)(H$_2$O)]·2H$_2$O (2·2H$_2$O). The addition of [Mn(3-MeOsalen)(H$_2$O)](ClO$_4$) (0.050 mmol) in MeOH/H_2O (1:1) to **1** (0.050 mmol) in MeOH produced a brown solution. This reaction mixture was stirred for 10 min, and then the filtrate was allowed to remain undisturbed, producing brown crystals in 70% yield. Elem anal. (%) calcd for $C_{40}H_{36}FeMnN_8O_8$: C, 55.4; H, 4.18; N, 12.9. Found: C, 55.6; H, 4.17; N, 12.6.

[Fe(qcq)(CN)$_3$][Mn(5-Clsalen)]·2MeOH (3·2MeOH). A solution of [Mn(5-Clsalen)(H$_2$O)]ClO$_4$ (0.050 mmol) in MeCN/H_2O (2:1) was added to **1** (0.050 mmol) in MeOH. After 10 min of stirring, the reaction solution was filtered and left undisturbed. Evaporation of the filtrate finally gave brown crystals suitable for X-ray, which were air-dried. Yield: 55%. Elem anal. (%) calcd for $C_{38}H_{30}Cl_2FeMnN_8O_6$ (**3**·3H$_2$O): C, 52.1; H, 3.45; N, 12.8. Found: C, 51.9; H, 3.22; N, 12.7.

[Fe(qcq)(CN)$_3$][Mn(5-Brsalen)]·2MeOH (4·2MeOH). To **1** (0.050 mmol) in MeOH was added a solution of [Mn(5-Brsalen)(H$_2$O)]ClO$_4$ (0.050 mmol) in MeCN/H_2O (2:1). The solution was reacted with stirring for 10 min. The filtrate was then slowly evaporated, producing brown crystals suitable for X-ray, which were air-dried. Yield: 57%. Elem anal. (%) calcd for $C_{40}H_{32}Br_2FeMnN_8O_5$: C, 49.3; H, 3.31; N, 11.5. Found: C, 49.3; H, 3.13; N, 11.4.

[Fe(qcq)(CN)$_3$][Mn(salen)]·MeCN (5·MeCN). A mixed solution of [Mn(salen)(H$_2$O)]ClO$_4$ (0.050 mmol) in MeCN/H_2O (1:1) was treated with **1** (0.050 mmol) in MeOH. Stirring of the reaction solution for 5 min was followed by filtration and slow evaporation. Brown crystals suitable for X-ray were precipitated over several days and were air-dried. Yield: 42%. Elem anal. (%) calcd for $C_{40}H_{31}FeMnN_9O_4$ (**5**·MeCN·H$_2$O): C, 59.1; H, 3.85; N, 15.5. Found: C, 59.6; H, 3.68; N, 15.2.

Physical Measurements. Elemental analyses for C, H, and N were performed at the Elemental Analysis Service Center of Sogang University. Infrared spectra were obtained from KBr pellets with a Bomen MB-104 spectrometer. Magnetic susceptibilities for **2**−**5** were carried out using a Quantum Design SQUID (dc) and a PPMS (ac) susceptometer. Diamagnetic corrections of **2**−**5** were estimated from Pascal's tables.

Crystallographic Structure Determination. X-ray data for **1**−**5** were collected on a Bruker SMART APEXII diffractometer equipped with graphite monochromated Mo Kα radiation (λ = 0.71073 Å). Preliminary orientation matrix and cell parameters were determined from three sets of ω scans at different starting angles. Data frames were obtained at scan intervals of 0.5° with an exposure time of 10 s per frame. The reflection data were corrected for Lorentz and polarization factors. Absorption corrections were carried out using SADABS.[17] The structures were solved by direct methods and refined by full-matrix least-squares analysis using anisotropic thermal parameters for non-hydrogen atoms with the SHELXTL program.[18] Lattice water molecules in **2** are significantly disordered and could not be modeled properly; thus, the program SQUEEZE,[19] a part of the PLATON package[20] of crystallographic software, was used to calculate the solvent disorder area and remove its contribution to the overall intensity data. All hydrogen atoms except for hydrogens bound to water molecules were calculated at idealized positions and refined with the riding models.

Results and Discussion

Synthesis and Characterization. A reaction of [Fe(qcq)(CN)$_3$]$^-$ and the corresponding Mn Schiff bases in a 1:1 stoichiometric ratio produced brown crystals of **2**−**5**. The mixed solvents used in the synthesis play a crucial role in making crystalline solids suitable for X-ray. The Cl−O stretching vibrations present at the starting Mn Schiff bases disappeared in the IR data of the products, implying that the 1:1 reactions were completed. The alteration of Mn Schiff bases led to the formation of the complexes with different types of structures or structural parameters, which are associated with the steric consequence of the side groups on the Schiff bases in the crystal packing. The IR spectra show that the characteristic CN bands are observed at 2123w (sh) and 2108m cm^{-1} for **1**, 2133m and 2116m cm^{-1} for **2**, 2130m and 2116m cm^{-1} for **3**, 2132m and 2117m cm^{-1} for **4**, and 2119m cm^{-1} for **5**. On the basis of the peaks of the precursor, one of the peaks for **2**−**5** significantly moves toward higher frequencies, indicating that CN ligands in the peak shift are involved in coordination to metal ions. The shift of the CN bands is related to the prevalent kinematic effect, which leads to restriction of the motion of CN groups, and electronic and geometric effects.[21]

Description of the Structures. The structures of **1**−**5** have been characterized using single-crystal X-ray diffraction techniques. Crystallographic data and the details of data collection for all of the complexes are listed in Table 1, and selected bond lengths and angles for **2**−**5** are summarized

(17) Sheldrick, G. M. *SADABS*; University of Göttingen: Göttingen, Germany, 1994.
(18) Sheldrick, G. M. *SHELXTL*, version 5; Bruker AXS: Madison, WI, 1995.
(19) van der Sluis, P.; Spek, A. L. *Acta Crystallogr.* **1990**, *A46*, 194.
(20) Spek, A. L. *Acta Crystallogr.* **1990**, *A46*, 1.
(21) Dunbar, K. R.; Heintz, R. A. *Prog. Inorg. Chem.* **1997**, *45*, 283.

Table 1. Crystallographic Data for **1**−**5**

	1	**2**	**3**·2MeOH	**4**·2MeOH	**5**·MeCN
formula	$C_{46}H_{32}FeN_6OP$	$C_{40}H_{32}FeMnN_8O_6$	$C_{40}H_{32}Cl_2FeMnN_8O_5$	$C_{40}H_{32}Br_2FeMnN_8O_5$	$C_{40}H_{29}FeMnN_9O_3$
fw	771.60	831.53	886.43	975.35	794.51
cryst syst	triclinic	triclinic	monoclinic	monoclinic	orthorhombic
space group	$P\bar{1}$	$P\bar{1}$	$P2_1/c$	$P2_1/c$	$P2_12_12_1$
temp (K)	293	293	130	130	130
a (Å)	9.3047(4)	13.961(3)	10.0113(3)	10.0064(2)	13.0638(4)
b (Å)	14.7946(7)	16.454(3)	14.1801(4)	14.2657(3)	13.5574(3)
c (Å)	14.8284(7)	19.703(4)	26.7347(7)	26.9395(7)	20.3649(5)
α (deg)	109.4130(10)	71.835(7)			
β (deg)	97.306(2)	74.846(7)	90.860(2)	90.805(2)	
γ (deg)	100.320(2)	69.937(7)			
V (Å^3)	1855.33(15)	3978.4(14)	3794.86(19)	3845.19(15)	3606.85(16)
Z	2	4	4	4	4
d_{calcd} (g cm^{-3})	1.381	1.388	1.552	1.685	1.463
μ (mm^{-1})	0.496	0.738	0.913	2.841	0.805
F(000)	798	1708	1812	1956	1628
reflns collected	19937	65988	35163	36828	17598
unique reflns	8208	19421	9207	9560	8484
goodness-of-fit	1.043	0.879	1.006	0.972	1.049
R1[a] [$I > 2\sigma(I)$]	0.1040	0.0533	0.0545	0.0613	0.0783
wR2[b] [$I > 2\sigma(I)$]	0.2168	0.1021	0.0996	0.1285	0.2121

[a] $R1 = \sum||F_o| - |F_c||/\sum|F_c|$. [b] $wR2 = [\sum w(F_o^2 - F_c^2)^2/\Sigma w(F_o^2)^2]^{1/2}$.

Table 2. Selected Bond Lengths (Å) and Angles (deg) for **2**−**5**

		2	
Fe−C_{bridge}	1.956(4)−1.960(3)	Fe−$C_{nonbridge}$	1.943(4)−1.969(4)
Fe−N	1.885(2)−2.027(3)	Mn−N_{bridge}	2.287(3)−2.289(3)
Mn−$O_{terminal}$	2.273(2)−2.324(2)		
Fe−C_{bridge}−N_{bridge}	174.2(3)−175.9(3)	Fe−$C_{nonbridge}$−$N_{nonbridge}$	173.2(3)−178.2(3)
Mn−N_{bridge}−C_{bridge}	144.6(2)−151.3(3)		
		3	
Fe(1)−C_{bridge}	1.930(4)−1.960(4)	Fe(1)−$C_{nonbridge}$	1.967(4)
Fe(1)−N	1.907(3)−2.009(3)	Mn(1)−N_{bridge}	2.280(3)−2.285(3)
Fe(1)−C_{bridge}−N_{bridge}	174.6(3)−176.2(3)	Fe(1)−$C_{nonbridge}$−$N_{nonbridge}$	177.2(3)
Mn(1)−N_{bridge}−C_{bridge}	147.7(3)−161.4(3)		
		4	
Fe(1)−C_{bridge}	1.926(7)−1.964(6)	Fe(1)−$C_{nonbridge}$	1.971(7)
Fe(1)−N	1.900(6)- 2.008(6)	Mn(1)−N_{bridge}	2.283(6)−2.291(5)
Fe(1)−C_{bridge}−N_{bridge}	175.0(5)−176.3(6)	Fe(1)−$C_{nonbridge}$−$N_{nonbridge}$	177.3(6)
Mn(1)−N_{bridge}−C_{bridge}	147.7(5)−159.9(5)		
		5	
Fe(1)−C_{bridge}	1.934(5)−1.970(5)	Fe(1)−$C_{nonbridge}$	1.960(6)
Fe(1)−N	1.889(6)−2.022(5)	Mn(1)−N_{bridge}	2.297(5)−2.298(5)
Fe(1)−C_{bridge}−N_{bridge}	174.1(5)−175.8(4)	Fe(1)−$C_{nonbridge}$−$N_{nonbridge}$	179.0(6)
Mn(1)−N_{bridge}−C_{bridge}	149.3(5)−153.5(5)		

in Table 2. The crystal structure of **1** is illustrated in Figure S1 (Supporting Information).

Complex 2. There exist two dimers within the unit cell with slightly different structural parameters. Figure 1 depicts a representative molecule within the cell of **2**. The dimeric unit is constructed from the anionic precursor $[Fe(qcq)(CN)_3]^-$ and the cationic $[Mn(3\text{-}MeOsalen)]^+$ part bridged by the cyanide ligand. The structural propagation is blocked by the coordination of one water molecule to one of the binding sites of the Mn Schiff base. In the crystal structure, the Fe geometry can be described as distorted octahedral, consisting of three C atoms from CN ligands and three N atoms from qcq. The mean Fe−C(cyanide) bond length is 1.95(1) Å. A strong σ-donor effect of the deprotonated amide is responsible for the shorter Fe−N(amide) bond distances [Fe1−N5 = 1.886(4) Å, Fe2−N13 = 1.900(4) Å] compared to those of the other Fe−N lengths ranging 1.982−2.027 Å.[12−15] The Fe−C−N angles remain almost linear, with the maximum deviations from 180° being 6.4° for Fe1 and 6.2° for Fe2. A Jahn−Teller distortion is evident, with a Mn octahedron judged by the shorter equatorial Mn−N(O) distances [mean Mn−N(O) = 1.93(6), 1.92(6) Å] than those of the apical Mn−N(O) distances [Mn1−N3 = 2.293(4) Å, Mn1−O6 = 2.275(3) Å, Mn2−N11 = 2.288(4) Å, Mn2−O12 = 2.323(3) Å]. The bridging Mn−N−C angles correspond to 145.0(3)° for Mn1−N3−C3 and 151.8(4)° for Mn2−N11−C43. The intrachain Fe−Mn distances through the CN linkage are 5.1243(14) Å for Fe1−Mn1 and 5.1841(15) Å for Fe2−Mn2.

In the extended structure of **2** (Figure 2), dimeric moieties are linked by hydrogen bonds among coordinated water molecules and oxygen atoms of methoxy and phenoxy groups (O···O = 2.854−3.096 Å) as well as $\pi-\pi$ interactions between aromatic rings of qcq ligands. The combination of

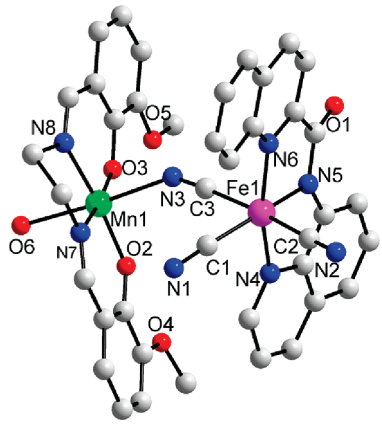

Figure 1. Molecular view of **2** with the selected atom-labeling scheme. The colors represent Fe in pink, Mn in green, N in blue, O in red, and C in gray.

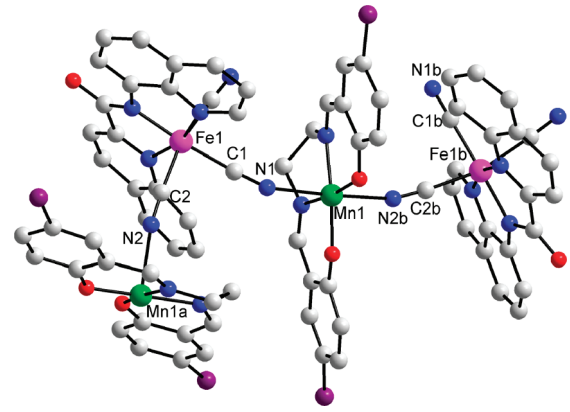

Figure 3. Molecular view of **3** with the selected atom-labeling scheme. Symmetry transformations used to generate equivalent atoms: $a = -x + 1, y - 0.5, -z + 0.5$; $b = -x + 1, y + 0.5, -z + 0.5$.

the noncovalent forces results in the construction of a two-dimensional (2D) architecture. The shortest interdimer M−M distances through the $\pi-\pi$ contacts are 8.577 Å for Fe1−Fe1, 9.066 Å for Fe2−Fe2, and 9.113 Å for Fe1−Fe2, while those via the hydrogen bonds are 4.842 Å for Mn1−Mn1and 4.943 Å for Mn2−Mn2.

Complexes 3 and 4. The structures of **3** and **4** can be seen as a zigzag chain formed by the precursor anion and the $[Mn(5\text{-}Xsalen)]^+$ (X = Cl and Br) cation (Figures 3 and 4). The bridging cyanides (C1−N1 and C2−N2) are used as bridges to Mn centers in a cis mode. The mean Fe−C(cyanide) bond length of 1.95(2)° for **3** and **4** is identical to **2**. The Fe−N(amide) bond distances are 1.907(3) Å for **3** and 1.900(6) Å for **4**, smaller than the other Fe−N lengths, which are concerned with a strong σ-donor effect of the deprotonated amide. The maximal deviations of the Fe−C−N angles from linearity are similar, 5.4° for **3** and 5° for **4**. The apparent disparity between the equatorial Mn−N(O) distances [mean Mn−N(O) = 1.94(6) Å for **3** and 1.95(6) Å for **4**] and axial Mn−N lengths [Mn1−N1 = 2.280(3) Å, Mn1a−N2 = 2.285(3) Å for **3** and Mn1−N2 = 2.291(5) Å and Mn1c−N1 = 2.283(6) Å for **4**; $a = 1 - x, -0.5 + y, 0.5 - z$; $c = -x, 0.5 + y, 0.5 - z$] demonstrates the presence of the Jahn−Teller effect of a Mn octahedron. The bridging Mn−N−C angles are 147.7(3)° for Mn1−N1−C1 and 161.4(3)° for Mn1a−N2−C2 (**3**) and 147.7(5)° for Mn1c−N1−C1 and 159.9(5)° for Mn1−N2−C2 (**4**). The intrachain Fe−Mn distances through the CN bridges are 5.1608(8) Å for Fe1−Mn1 and 5.2978(8) Å for Fe1−Mn1a (**3**) and 5.1616(13) Å for Fe1−Mn1 and 5.2950(12) Å for Fe1−Mn1c (**4**).

The extended structures of **3** and **4** are established by $\pi-\pi$ contacts between benzene rings of aminoquinoline groups of qcq on adjacent chains (Figures 5 and S2). The centroid distances are 3.672 Å for **3** and 3.625 Å for **4**. The shortest Fe−Fe distance through the noncovalent interactions is 8.992 Å for **3** and 9.024 Å for **4**. Hydrogen bonds among OH

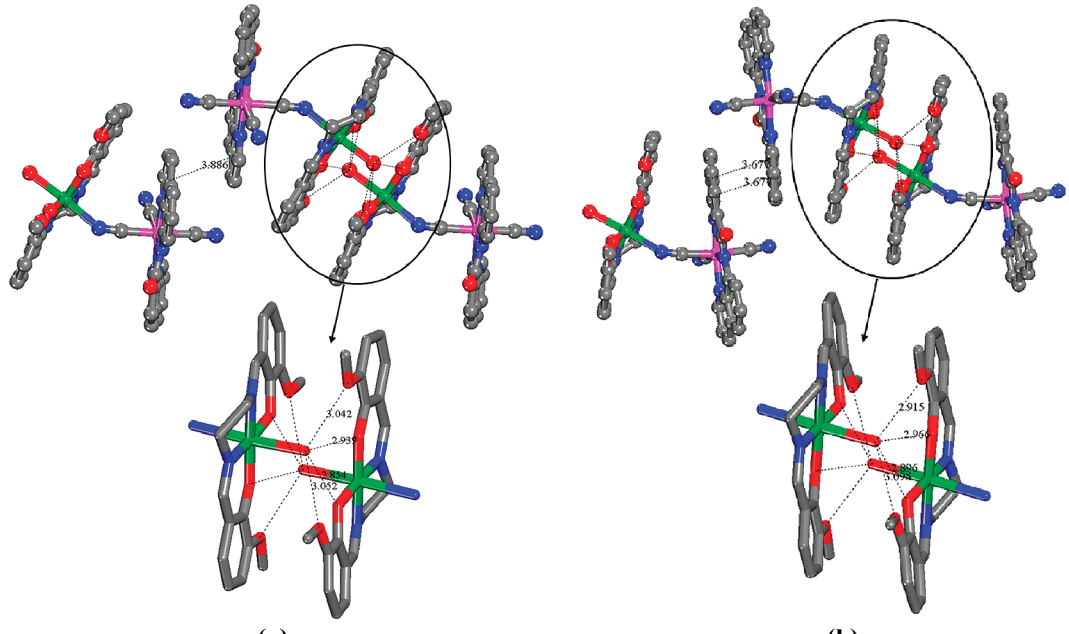

Figure 2. Extended structure of **2** displaying $\pi-\pi$ interactions between quinoline rings present in adjacent dimers as well as hydrogen bonds between coordinated water molecules and oxygen groups of the Schiff bases.

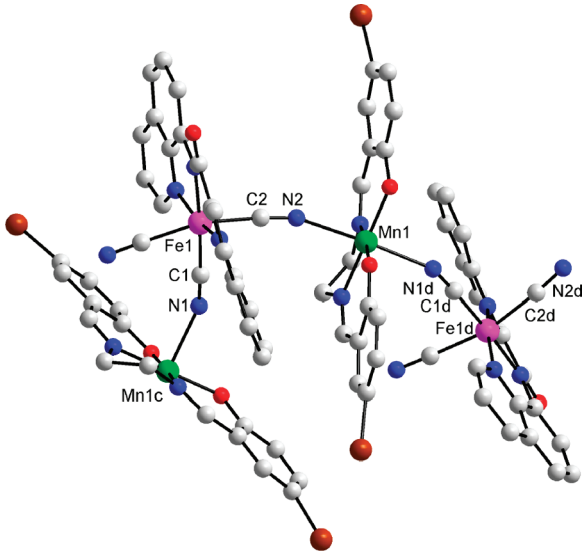

Figure 4. Molecular view of **4** with the selected atom-labeling scheme. Symmetry transformations used to generate equivalent atoms: $c = -x, y + 0.5, -z + 0.5$; $d = -x, y - 0.5, -z + 0.5$.

groups of methanols and oxygens of carbonyl groups on qcq are present.

Complex 5. The structure of **5** comprises the Fe tricyanide precursor and the $[Mn(salen)]^+$ moiety (Figure 6). Unlike **2**, the use of salen without methoxy groups in the 3- position of the Schiff base affords a zigzag chain, which is generated by the coordination of two cyanides (C1−N1 and C3−N3) in a cis mode to Mn centers. It is noted that the presence or absence of the side groups (Cl or Br) on salen in the 5-position does not change the overall chain structure. The mean Fe−C(cyanide) bond length of 1.95(2) Å for **5** is the same as that for **2**. The shorter Fe−N(amide) bond distances of Fe1−N5 = 1.889(6) Å than those of the other Fe−N lengths are due to a strong σ-donor effect of the deprotonated amide. The maximal deviation of the Fe−C−N angles from linearity is 5.9° for Fe1. The short equatorial Mn−N(O) distances [mean Mn−N(O) = 1.94(6) Å] and the elongated apical Mn−N(O) distances [Mn1−N3 = 2.298(5) Å and Mn1e−N1 = 2.297(5) Å; $e = 0.5 + x, 0.5 - y, -z$] arise from the Jahn−Teller distortion of a Mn octahedron. The Mn−N−C angles in the bridging pathways are equal to 153.5(5)° for Mn1−N3−C3 and 149.3(5)° for Mn1e−N1−C1. The intrachain Fe−Mn distances through the CN bridges are 5.2276(13) Å for Fe1−Mn1 and 5.2015(12) Å for Fe1−Mn1e.

The overall structure of **5** in the crystal packing is formed by extensive $\pi-\pi$ interactions between chains (Figure 7). In the view generated in the direction of the arrow, the $\pi-\pi$ interactions between benzene rings of 8-aminoquinoline groups and pyridyl rings of quinoline groups bring about the construction of a 2D layer (Figure 7b). The centroid distance through the contacts is 3.586 Å, and the shortest Fe−Fe distance is 8.158 Å. In the other view in the direction of the arrow, a 2D sheet is built up with the $\pi-\pi$ stackings of different types of quinoline rings residing in nearby chains (Figure 7c). The coordinative and noncovalent bonds eventually give rise to a 3D network structure.

Magnetic Properties of 1. The magnetic data of **1** were collected in the temperature range 2−300 K and 1000 G, as depicted in Figure S3 (Supporting Information). The $\chi_m T$ value is equal to 0.786 cm^3 K mol^{-1} at 300 K, which is much larger than the spin-only value (0.375 cm^3 K mol^{-1}) for a noncoupled $S_{Fe} = 1/2$ but consistent with those reported for low-spin Fe(III) analogues.[14,22a] The $\chi_m T$ behavior on lowering the temperature is typical of octahedral low-spin Fe(III) systems with the $^2T_{2g}$ ground term.[14,22]

Magnetic Properties of 2. The magnetic susceptibility data per FeMn of **2** were measured at a field of 1000 G and temperatures of 2−300 K, as shown in Figure 8. The $\chi_m T$ value at 300 K is 3.18 cm^3 K mol^{-1}, which is slightly smaller than the spin-only one (3.38 cm^3 K mol^{-1}) expected for independent Fe^{III} ($S_{Fe} = 1/2$) and Mn^{III} spins ($S_{Mn} = 2$). A slow decrease in $\chi_m T$ designates the operation of antiferromagnetic interactions between the magnetic centers. The high-temperature data ($T > 10$ K) were fitted using the

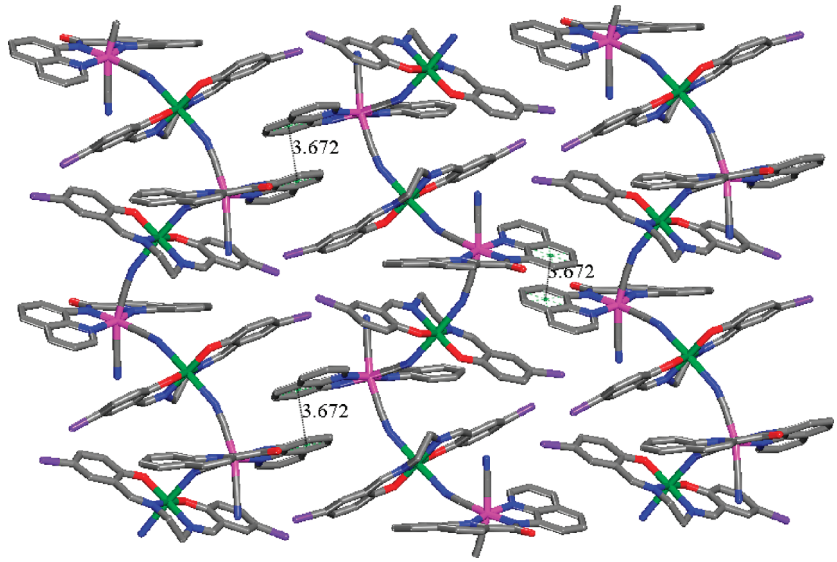

Figure 5. Extended 2D structure of **3** incorporating $\pi-\pi$ contacts between benzene rings of aminoquinoline groups of qcq with a centroid distance of 3.672 Å. The shortest Fe−Fe distance through the noncovalent interactions is 8.992 Å.

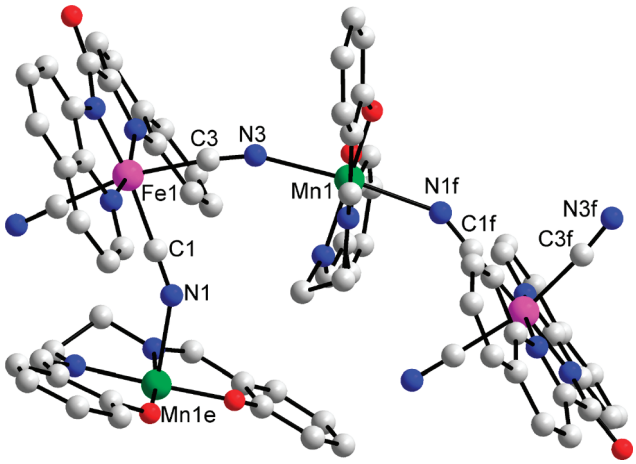

Figure 6. Molecular view of **5** with the selected atom-labeling scheme. Symmetry transformations used to generate equivalent atoms: $e = x + 0.5, -y + 0.5, -z$; $f = x - 0.5, -y + 0.5, -z$.

Curie−Weiss law to give $C = 3.29$ cm^3 K mol^{-1} and $\theta = -11.1$ K, supporting the idea that dominant antiferromagnetic couplings mediate between the metal ions.

Application of a dimer model ($H = -JS_{Mn} \cdot S_{Fe}$) under consideration of the interdimer interactions (zJ') to the data ($T > 7$ K) yielded magnetic parameters of $g = 1.96$, $J = -9.3$ cm^{-1}, and $zJ' = -0.95$ cm^{-1}.

$$\chi = (Ng^2\beta^2/3kT)[A/B]$$
$$A = 15 + 52.5\exp(2.5x), B = 4 + 6\exp(2.5x), x = J/kT$$
$$\chi_m = \chi/(1 - zJ'\chi/Ng^2\beta^2) \quad (1)$$

Inclusion of zero-field splitting parameter (D) was attempted using the MAGPACK program,[23] which provided a minimal D value of less than 0.01 cm^{-1} with no virtual changes in the other parameters. The observed magnetic exchange value reveals the presence of intrachain antiferromagnetic interactions between Mn^{III} and Fe^{III} ions via the CN bridges, which is consistent with the Fe^{III}−Mn^{III} systems made of *mer*-Fe tricyanides[14,15] but different from other analogous Fe^{III}−Mn^{III} bimetallic systems exhibiting ferromagnetic alignments.[24] It is evident that antiferromagnetic interactions (zJ') occur between dimeric units, which are relevant with the presence of the $\pi-\pi$ contacts and hydrogen bonds in **2**. As shown in the inset of Figure 8, the $M(H)$ data reveal that the experimental data are substantially below the Brillouin curves derived from noncoupled spins within a dimer (dashed line) and the intradimer antiferromagnetic consequence of $S = S_{Mn} - S_{Fe} = 3/2$ (solid line). These results demonstrate that prevalent antiferromagnetic interactions are transmitted within a dimer and between dimers.

Magnetic Properties of 3 and 4. The magnetic susceptibility data of **3** and **4** were collected at 1000 G in the temperature range from 2 to 300 K, as shown in Figures 9 and 10, respectively. The $\chi_m T$ values at 300 K are 3.56 cm^3 K mol^{-1} (**3**) and 3.50 cm^3 K mol^{-1} (**4**), which are a little larger than the theoretical value calculated from the magnetically dilute two-spin system (S_{Fe}, S_{Mn}) = (1/2, 2). As the temperature is lowered, $\chi_m T$ decreases slowly and arrives at a minimum of 2.42 cm^3 K mol^{-1} and 2.18 cm^3 K mol^{-1} at $T_{min} = 20$ K for **3** and **4**, respectively. Below T_{min}, the $\chi_m T$ product increases up to 5.11 cm^3 K mol^{-1} for **3** and 6.35 cm^3 K mol^{-1} for **4** at 2 K. The overall magnetic behavior resembles that of **3**, typical of a ferrimagnetic situation within a chain.[25] The high-temperature data of $T > 30$ K obeys the Curie−Weiss law with $C = 3.57$ cm^3 K mol^{-1} and $\theta = -15.6$ K (**3**) and $C = 3.32$ cm^3 K mol^{-1} and $\theta = -19.5$ K (**4**), supporting the existence of antiferromagnetic couplings between the paramagnetic centers.

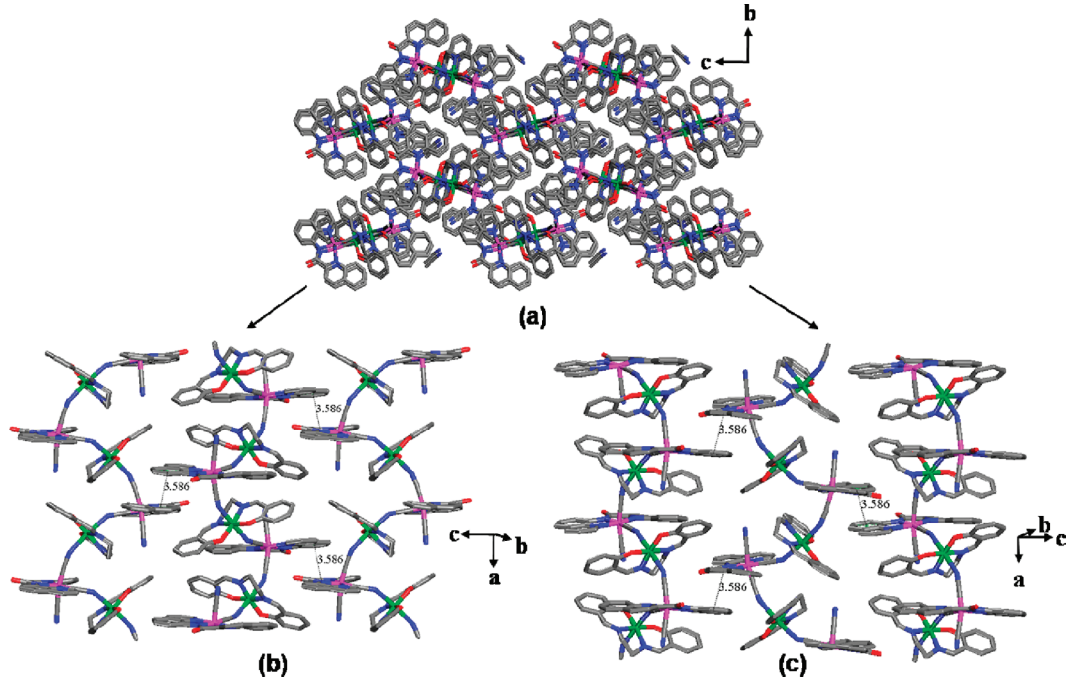

Figure 7. (a) Extended 3D structure of **5** formed by $\pi-\pi$ interactions between chains. Parts b and c show 2D sheets constructed by coordinative 1D chains and additional $\pi-\pi$ stackings.

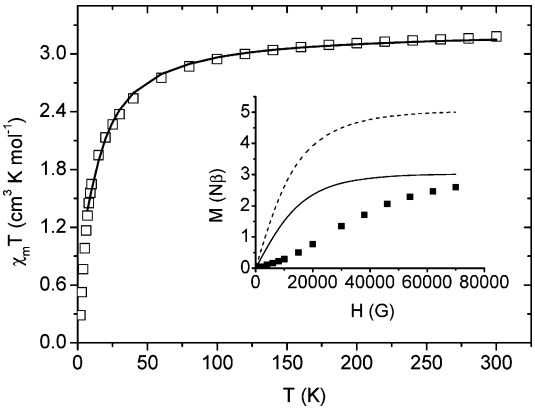

Figure 8. Plots of $\chi_m T$ versus T at 0.1 T (main panel) and magnetization vs H at 2 K (inset) for **2**. The solid line in the main panel represents the computed curve. The Brillouin curves derived from noninteracting magnetic spins (dashed line) and $S = 3/2$ (solid line) with $g = 2$ are shown in the inset.

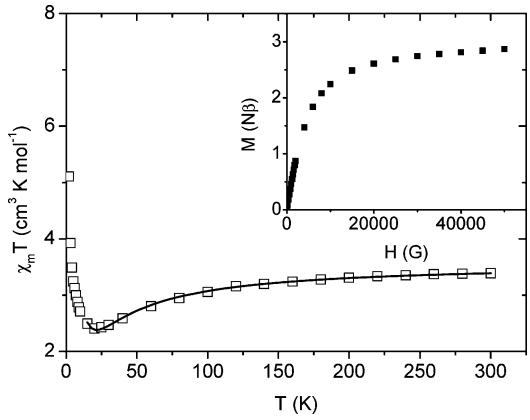

Figure 9. Plots of $\chi_m T$ vs T at 0.1 T (main panel) and magnetization vs H at 2 K (inset) for **3**. The solid line gives the fitted curve.

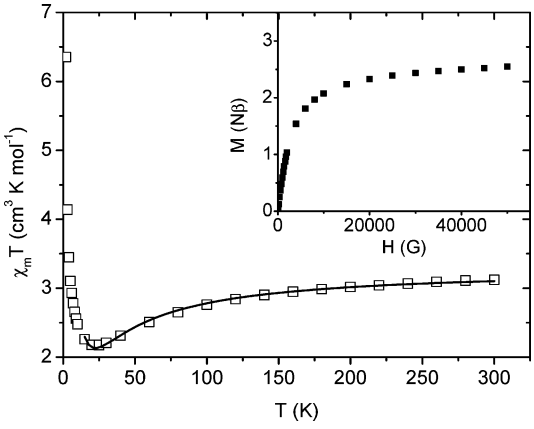

Figure 10. Plots of $\chi_m T$ vs T at 0.1 T (main panel) and magnetization vs H at 2 K (inset) for **4**. The solid line gives the fitted curve.

We used the ferrimagnetic chain model to probe the magnetic exchange coupling.[26] Fits were carried out with magnetic data in the temperature range 15−300 K to preclude Zeeman effect, zero-field splitting, and interchain magnetic interactions.[14,15,27]

$$\chi_m T = \frac{N\beta^2}{3k}\left[g^2\frac{1+u}{1-u} + \delta^2\frac{1-u}{1+u}\right] \qquad (2)$$

The parameters are as follows: $g_{Mn}{}^e = g_{Mn}[S_{Mn}(S_{Mn}+1)]^{1/2}$, $g_{Fe}{}^e = g_{Fe}[S_{Fe}(S_{Fe}+1)]^{1/2}$, $J^e = J[S_{Mn}(S_{Mn}+1)S_{Fe}(S_{Fe}+1)]^{1/2}$, $g = (g_{Mn}{}^e + g_{Fe}{}^e)/2$, $\delta = (g_{Mn}{}^e - g_{Fe}{}^e)/2$, $u = \coth(J^e/kT) - (kT/J^e)$. The least-squares fittings conferred roughly estimated parameters of $g_{Mn} = 1.99$, $g_{Fe} = 2.52$, and $J = -10.5$ cm^{-1} for **3** and $g_{Mn} = 1.90$, $g_{Fe} = 2.48$, and $J = -11.8$ cm^{-1} for **4**.[11e,28] The intrachain antiferromagnetic characters observed in **3** and **4** are consistent with those for **2** and other $Fe^{III}-Mn^{III}$ assemblies based on *mer*-Fe tricyanide precursors.[14,15] The field dependence of the magnetization at 2 K was recorded in the field range from 0 to 5 T, as illustrated in the insets of Figures 9 and 10. The magnetization values at 5 T correspond to 2.87 Nβ for **3** and 2.55 Nβ for **4**, which are smaller than the ferrimagnetic results of 3 Nβ calculated from $M_S = g(S_{Mn} - S_{Fe})$ with $g = 2$. The low saturation magnetization is related to the Mn^{III} anisotropy.

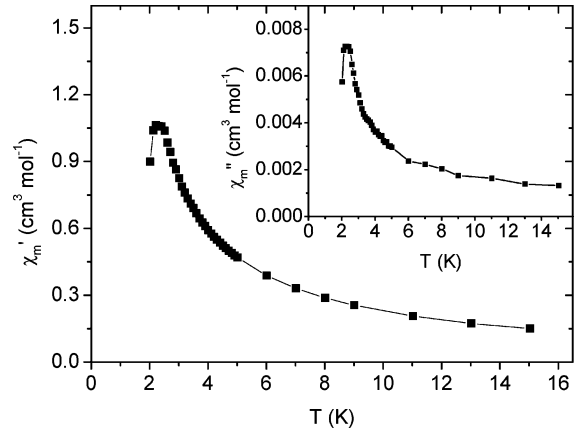

Figure 11. Plots of in-phase (χ_m'' in main panel) and out-of-phase (χ_m' in inset) components of ac magnetic susceptibility data measured at an ac field of 5 G and an oscillating frequency of 3000 Hz for **3**.

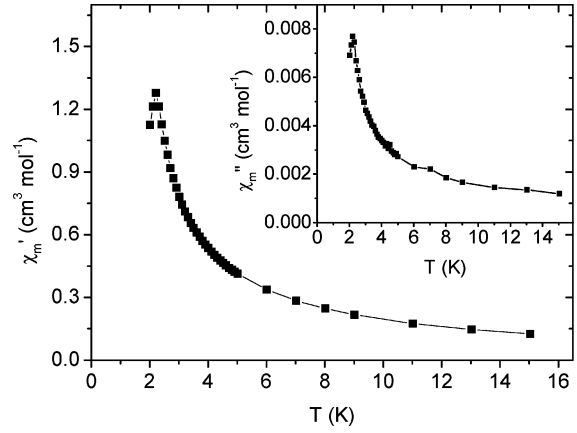

Figure 12. Plots of in-phase (χ_m'' in main panel) and out-of-phase (χ_m' in inset) components of ac magnetic susceptibility data for **4**.

The ac magnetic susceptibility data in Figures 11 and 12 were examined at an ac field of 5 G and 3000 Hz. The frequency dependences in the ac plots are not visible in **3** and **4**. Noticeably, an obvious signal of the in-phase component (χ_m') is observed at 2.3 K for **3** and 2.2 K for **4**, respectively, which are accompanied by peaks of the out-of-phase part (χ_m'') in the ac data. This magnetic feature is the signature of a long-range order in both complexes and

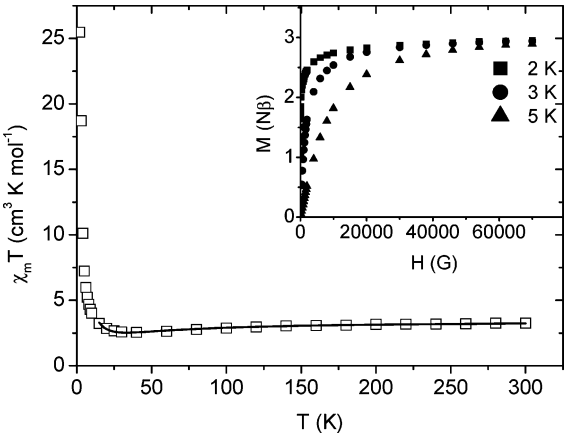

Figure 13. Plots of $\chi_m T$ vs T at 0.1 T (main panel) and magnetization vs H at indicated temperatures (inset) for **5**. The solid line gives the fitted curve.

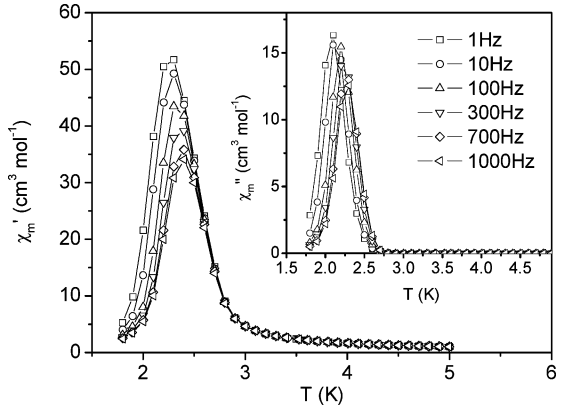

Figure 14. Plots of χ_m' and χ_m'' (inset) versus T of **5** at an ac field of 3 G, zero dc field, and several indicated frequencies.

can be understood in terms of enhanced magnetic couplings between chains through the noncovalent interactions.[29]

Magnetic Properties of 5. The temperature dependence of the magnetic susceptibility data per FeMn of **5** in the temperature range 2−300 K is plotted in Figure 13. The $\chi_m T$ value of 3.25 cm^3 K mol^{-1} at 300 K is somewhat smaller than the spin-only one (3.38 cm^3 K mol^{-1}) anticipated from noninteracting Fe^{III} ($S_{Fe} = 1/2$) and Mn^{III} spins ($S_{Mn} = 2$). A gradual decay in $\chi_m T$ supports the idea that antiferromagnetic interactions take place between Fe^{III} and Mn^{III} spins. The $\chi_m T$ product reaches a minimum of 2.54 cm^3 K mol^{-1} at $T_{min} = 40$ K and then undergoes a sharp rise to 25.5 cm^3 K mol^{-1} at 2 K. This behavior is characteristic of a ferrimagnetic arrangement resulting from the noncompensation of two antiferromagnetically coupled spins. The higher value of T_{min} for **5** than those for **3** and **4** suggests that intrachain antiferromagnetic interactions of **5** are stronger than those of **3** and **4**. The overall antiferromagnetic couplings in the high-temperature range are confirmed by the Curie−Weiss fitting to temperatures of $T > 40$ K, resulting in $C = 3.57$ cm^3 K mol^{-1} and $\theta = -20.8$ K.

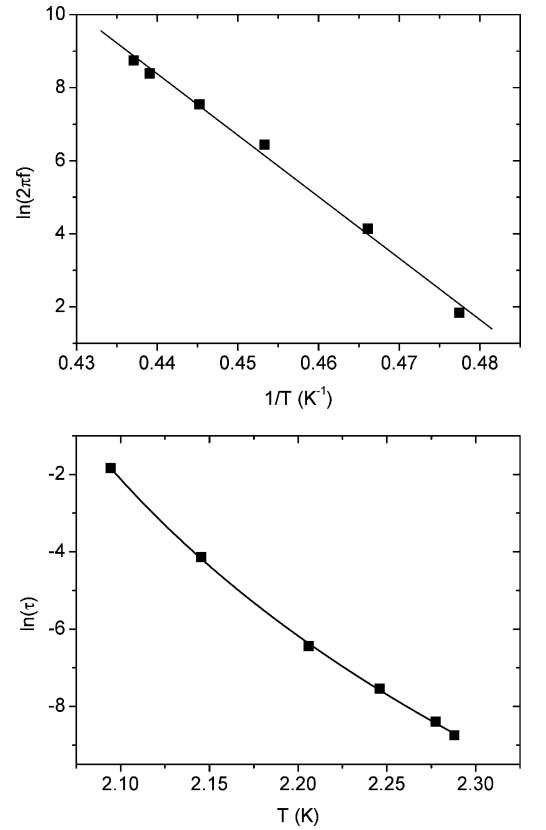

Figure 15. Plots of relaxation rate versus reciprocal temperature (top) and ln(τ) versus temperature (bottom) for **5**. The solid lines represent the best fits of the data to the Arrhenius equation and critical slowing-down equation, respectively.

An analytical expression for the regular ferrimagnetic chain system was employed in the temperature range 15−300 K.[26] The roughly estimated result is equal to $g_{Mn} = 1.99$, $g_{Fe} = 2.20$, and $J = -14.1$ cm^{-1}.[28] The negative value of J indicates that antiferromagnetic couplings are operating between Fe^{III} and Mn^{III} through the cyanide bridge. As seen in the inset of Figure 13, the $M(H)$ value of 2.94 Nβ at a field of 7 T and temperatures of 2, 3, and 5 K shows that the saturation magnetization is close to the ferrimagnetic consequence of $gS = g(S_{Mn} - S_{Fe}) = 3$ Nβ assuming $g = 2$.

The thermal variation of the ac magnetic susceptibility for **5** was inspected at zero dc field, an ac field of 3 G, and

(22) (a) Lescouëzec, R.; Lloret, F.; Julve, M.; Vaissermann, J.; Verdaguer, M.; Llusar, R.; Uriel, S. *Inorg. Chem.* **2001**, *40*, 2065. (b) Toma, L. M.; Lescouëzec, R.; Toma, L. D.; Lloret, F.; Julve, M.; Vaissermann, J.; Andruh, M. *J. Chem. Soc., Dalton Trans.* **2002**, 3171.
(23) Borras-Almenar, J. J.; Clemente-Juan, J. M.; Coronado, E.; Tsukerblat, B. S. *J. Comput. Chem.* **2001**, *22*, 985.
(24) (a) Miyasaka, H.; Ieda, H.; Matsumoto, N.; Re, N.; Crescenzi, R.; Floriani, C. *Inorg. Chem.* **1998**, *37*, 255. (b) Miyasaka, H.; Matsumoto, N.; Re, N.; Gallo, E.; Floriani, C. *Inorg. Chem.* **1997**, *36*, 670. (c) Ni, Z.-H.; Kou, H.-Z.; Zhang, L.-F.; Ge, C.; Cui, A.-L.; Wang, R.-J.; Li, Y.; Sato, O. *Angew. Chem., Int. Ed.* **2005**, *44*, 7742. (d) Ni, Z.-H.; Zhang, L.-F.; Tangoulis, V.; Wernsdorfer, W.; Cui, A.-L.; Sato, O.; Kou, H.-Z. *Inorg. Chem.* **2007**, *46*, 6029. (e) Choi, H. J.; Sokol, J. J.; Long, J. R. *J. Phys. Chem. Solids* **2004**, *65*, 839. (f) Miyasaka, H.; Saitoh, A.; Abe, S. *Coord. Chem. Rev.* **2007**, *251*, 2622.
(25) Yoon, J. H.; Kim, H. C.; Hong, C. S. *Inorg. Chem.* **2005**, *44*, 7714.
(26) Drillon, M.; Coronado, E.; Beltran, D.; Georges, R. *Chem. Phys.* **1983**, *79*, 449.
(27) (a) Zhang, Y.-Z.; Gao, S.; Wang, Z.-M.; Su, G.; Sun, H.-L.; Pan, F. *Inorg. Chem.* **2005**, *44*, 4534. (b) Yang, C.-I.; Wernsdorfer, W.; Lee, G.-H.; Tsai, H.-L. *J. Am. Chem. Soc.* **2007**, *129*, 456.
(28) Given that Mn^{III} and Fe^{III} spins are antiparallel, Mn^{III} was assumed to act as a classical spin carrier with $S_{Mn} = 2$, leading to an effective alternating chain with $S_{Mn} = 2$ and $S_{Fe} = 1/2$. The magnetic model may be roughly applied to the system with the quantum spin $S_{Fe} = 1/2$.
(29) Kou, H.-Z.; Gao, S.; Ma, B.-Q.; Liao, D.-Z. *Chem. Commun.* **2000**, 713.

Table 3. Specific Structural Parameters ($Mn-N_{cyano}$ Lengths and $Mn-C\equiv N$ Angles in the Bridging Pathways) and Related Magnetic Coupling Constants for Fe(III)−Mn(III) Systems Constructed from *mer*-Fe^{III} Tricyanides

compounds	structure	$Mn-N_{cyano}$ (Å)	$Mn-N\equiv C$ (deg)	J (cm^{-1})	ref
a	dimer	2.275(3)	164.1(2)	−17.2	15
2	dimer	2.289(3), 2.287(3)	144.6(2), 151.3(3)	−9.3	this work
b	1D chain	2.283(3), 2.263(3)	152.2(3), 158.3(3)	−17.2	14
c	1D chain	2.287(5), 2.298(5)	169.1(4), 154.3(5)	−6.5	15
3	1D chain	2.280(3), 2.285(3)	147.7(3), 161.4(3)	−10.5	this work
4	1D chain	2.283(6), 2.291(5)	147.7(5), 159.9(5)	−11.8	this work
5	1D chain	2.297(5), 2.298(5)	149.3(5), 153.5(5)	−14.1	this work

[a] $[Fe(mpzcq)(CN)_3][Mn(salen)(H_2O)]\cdot H_2O$. [b] $[Fe(pzcq)(CN)_3][Mn(salen)]\cdot 4H_2O$. [c] $[Fe(mpzcq)(CN)_3][Mn(salcy)]\cdot MeOH\cdot MeCN$.

oscillating frequencies from 1 to 1000 Hz (Figure 14). The in-phase component (χ_m') and out-of-phase part (χ_m'') in the ac data definitely disclose the frequency dependence of the maxima in the plots. The spin relaxation can be characterized using the quantitative measure equated as $\phi = \Delta T_{max}/T_{max}\Delta(\log \omega)$ in which T_{max} is the peak temperature in χ_m' and ω is the angular frequency. The calculated value of ϕ is 0.018, which falls into canonical spin glasses.[30] As shown in the top panel of Figure 15, we applied the Arrhenius law [$\tau = \tau_0 \exp(\Delta/k_BT)$] to the χ_m'' data, where τ stands for the relaxation time, τ_0 the pre-exponential factor, and Δ the energy barrier. The fitting result affords $\tau_0 = 2.4 \times 10^{-36}$ s and $\Delta/k_B = 168$ K. The obtained τ_0 value is quite small when compared with those of typical SCMs.[8] The frequency-dependent maxima in χ_m'', often taken as a sign of a spin glass system, are fitted to the dynamical slowing down for spin glasses expressed as $\tau/\tau_0 = [T_f/T_G - 1]^{-z\nu}$, where τ is the relaxation time, T_f the freezing temperature, T_G the spin glass temperature, and $z\nu$ the critical exponent. The bottom panel of Figure 15 points out that the best fit affords parameters of $\tau_0 = 3.5 \times 10^{-11}$ s, $T_G = 1.9$ K, and $z\nu = 9.4$. The obtained τ_0 falls into the category of spin glasses, and the $z\nu$ value also conforms to the range from 4 to 12 of canonical spin glasses.[30,31] This characteristic reflects a glassy state imbedded in **5**. Compared with related extended structures and magnetic natures of **3** and **4**, a long-range magnetic order in **5** may not be ruled out. Such glassy behavior is likely associated with the single-ion anisotropy, interchain magnetic interactions (dipolar or exchange coupling), or some changes in solvent content. Similar behavior was found in a 1D chain complex [Mn^{III}TBrPP][TCNE] where both magnetic competition between different magnetic states on neighboring chains and partial solvent disorder/loss were suggested to be the source of frustration and randomness for spin glasses.[32]

Magnetostructural Correlation. First of all, a simple orbital scheme is considered to account for the underlying magnetic natures of the prepared $Fe^{III}-Mn^{III}$ compounds. The total exchange coupling constant (J) can be provided by the summation of the ferromagnetic term (J_F) and the antiferromagnetic term (J_{AF}) proportional to the overlap integral.[33] On the basis of the DFT calculations conducted on the *mer*-$[Fe(qcq)(CN)_3]^-$ precursor (Figure S5, Supporting Information), which are similar to the results for the *mer*-$[Fe(bpca)(CN)_3]^-$ complex,[12] the main magnetic orbital of *mer*-$[Fe(qcq)(CN)_3]^-$ in the present system may be a d_{xz} orbital residing in the tricyanide plane where the x and z axes pass through the N(5)−Fe(1)−C(1) and C2−Fe(1)−C(3) vectors. Because all of the known $Fe^{III}-Mn^{III}$ examples bearing *mer*-Fe(III) tricyanides indicate antiferromagnetic interactions via cyanide bridges (Table 3), which are contrary to most cyanide-linked $Fe^{III}-Mn^{III}$ bimetallic systems,[24] it seems reasonable that the orbital overlaps in this system, which can occur between an Fe^{III} d_{xz} orbital and Mn^{III} $d\pi$ orbitals, are effective.[24] This antiferromagnetic contribution from the orbital overlap should overcome the ferromagnetic contribution primarily from Fe d_{xz}−Mn d_{z^2} routes to give the observed overall antiferromagnetic character in this system. The factors, which affect the strength of the magnetic exchange coupling, appear to be rather complicated; the combined effects from the Mn−N(axial) bond lengths, the bending of the $Mn-N\equiv C-Fe$ skeletons, and the rotation of the x and z axes for Mn(III) with respect to the xz plane should be taken into consideration. For the dimeric systems, it is manifest that the bending of the $Mn-N\equiv C$ angles plays a crucial role in diminishing the overlap and then reducing the antiferromagnetic couplings. In contrast, the structural parameters of the Mn−N(axial) lengths and $Mn-N\equiv C$ angles in the 1D materials are varied, and their magnetic strengths are irregular. Therefore, all of the aforementioned factors may be delicately incorporated in the magnetic results of the current 1D family.

Conclusions

We have prepared the dimeric (**2**) and 1D chain complexes (**3**−**5**) by using a newly made molecular precursor [Fe(qcq)$(CN)_3]^-$ (**1**) with a meridional arrangement. The involvement of noncovalent stackings (hydrogen bonding and $\pi-\pi$ contact) causes the construction of higher-dimensional architectures. The magnetic data for all of the prepared compounds undoubtedly reveal the operation of antiferromagnetic interactions between Fe^{III} and Mn^{III} centers mediated by cyanide bridges, which may be assigned to the enhanced orbital overlap in the systems constructed from the *mer*-Fe^{III} tricyanides. The bending of the $Mn-N\equiv C$

(30) Mydosh, J. A. *Spin Glasses, An Experimental Introduction*, Taylor & Francis: London, 1993; pp 64−76.
(31) (a) Greedan, J. E.; Raju, N. P.; Maignan, A.; Simon, Ch.; Pedersen, J. S.; Niraimathi, A. M.; Gmelin, E.; Subramanian, M. A. *Phys. Rev. B: Condens. Matter Mater. Phys.* **1996**, *54*, 7189. (b) Laiho, R.; Lahderanta, E.; Salminen, J.; Lisunov, K. G.; Zakhvalinskii, V. S. *Phys. Rev. B: Condens. Matter Mater. Phys.* **2001**, *63*, 094405. (c) Tholence, J. L. *Physica B* **1984**, *126*, 157. (d) Hong, C. S.; Kim, W. S.; Chi, E. O.; Hur, N. H.; Choi, Y. N. *Chem. Mater.* **2002**, *14*, 1832.
(32) Rittenberg, D. K.; Sugiura, K.-i.; Sakata, Y.; Mikami, S.; Epstein, A. J.; Miller, J. S. *Adv. Mater.* **2000**, *12*, 126.
(33) Kahn, O. *Molecular Magnetism*; VCH: Weinheim, Germany, 1993.

angles obviously affects the magnetic strengths in the dimers; however, the other structural parameters may be also taken into account to understand the magnetic properties of the 1D chain complexes.

Acknowledgment. This work was supported by a Korea Science and Engineering Foundation (KOSEF) grant (No. R01-2007-000-10240-0) and Nuclear R&D Programs funded by the Korea government (MOST). Work at Sungkyunkwan University was supported by the Acceleration Research Program (Grant No. R17-2008-033-01000-0) and the Global Research Network Program.

Supporting Information Available: X-ray crystallographic files in CIF format for **1**−**5**, additional structural and magnetic data, and magnetic analyses for the complexes. This material is available free of charge via the Internet at http://pubs.acs.org.

IC802033Q